MiGriBot: A Miniature Parallel Robot with Integrated Gripping for High Throughput Micromanipulation

Maxence Leveziel[1], Wissem Haouas[1], Guillaume J. Laurent[1],

Michaël Gauthier[1], Redwan Dahmouche[1*]

[1]FEMTO-ST Institute, CNRS, Univ. Bourgogne Franche-Comté

24 rue Alain Savary, F-25000 Besançon, France

*To whom correspondence should be addressed; E-mail: redwan.dahmouche@femto-st.fr

Although robotic micromanipulation using microtweezers has widely been explored, the current manipulation throughput hardly exceeds one operation per second. Increasing the manipulation throughput is thus a key factor for the emergence of robotized micro-assembly industries. This article presents the MiGriBot, a miniaturized parallel robot with a configurable platform and soft joints, designed to perform pick-and-place operations at the microscale. MiGriBot combines in a single robot the benefits of an original parallel kinematic architecture with a configurable platform and a millimeter-scale compliant mechanism. Indeed, the configurable platform of the robot provides an internal degree of freedom used to actuate a microtweezers using piezoelectric bending actuators located at the base of the robot, which significantly reduces

the robot's inertia, while the soft joints allow to miniaturize the mechanism and to avoid friction. These benefits enable MiGriBot to reach the unprecedented throughput of 10 pick-and-place cycles per second of micro-objects and a positioning repeatability down to a micron.

Introduction

Increasing the throughput of robotic manipulators has been a challenge for decades to reduce the production cost and to improve the volume of production. The need is even greater at small scale where the level of production (e.g. MEMS, microelectronics) is huge. Recent works in microrobotics pave the way to the development of miniaturized parallel manipulators whose low moving mass makes it possible to reach unequalled speeds for contact-based micromanipulation. One of the groundbreaking results is the Millidelta (*1*) which is a Delta-like miniaturized parallel robot able to perform very high-speed trajectories such as circles with a frequency up to 75 Hz. Indeed, parallel kinematic architectures (*2*) have several benefits compared to serial ones. First, the actuators can be fixed on the robot's base leading to lighter moving parts. In addition, the moving platform is more rigid than its serial counterpart for an equivalent moving mass. The combination of the high rigidity and light moving parts increases the natural frequencies of the robot's structure and allows for high-speed positioning capabilities. One of the most common parallel architecture that illustrates these benefits is the Delta robot (*3, 4*), which has three translational Degrees-of-Freedom (DoF). Its high-speed makes it particularly suitable where high throughput pick-and-place operations are required such as in the electronics industry (*5*).

Another advantage of parallel robot structures is that they can generate controlled rotations from linear actuators. The combination of micro-transducers that are able to generate

high-speed translations, such as piezo-stacks and piezo-benders (*6, 7*), with lightweight parallel structures can then allow to obtain several DoF and reach very short response times. However, since classical spherical, universal and revolute joints cannot be miniaturized under a certain level, they are replaced by flexure hinges. The resulting benefit is that, contrarily to classical mechanisms, compliant structures do not introduce backlash and friction in the mechanism. Sub-micrometer repeatability can thus be reached using this class of structures (*8, 9*).

Compliant joints are usually obtained through notch hinges and leaf spring hinges in a single piece of material. However, the deformation amplitude of such joints is small and considerably limits the workspace of the robots (*10–12*). A possible way to enlarge the workspace is to make the links wholly deformable which leads to parallel continuum robots (*13–15*). However, developing accurate models for these classes of robots is complex and their inversion is time consuming leading to low frequency control loops (*16–19*).

Another solution is to use a combination of hard and soft materials to obtain the desired soft joint behavior. For revolute joints, the preferred technique is to laminate a rigid layer for the rigid links with a flexible layer for the hinges (*20*). The lamination is most of the time done with carbon fiber sheet as rigid links and polyimide film for the flexure part. The milliDelta and many miniature mechanisms rely on this technique with different materials (*1, 21–23*). Spherical joints can be obtained using elastomeric parts between rigid links (*24, 25*). These soft joints can be realized through photolithography (*26, 27*) or by molding in silicon micro-structures (*28*).

The predominant issue of the current parallel miniaturized robots is the lack of grasping abilities (*29, 30*). Indeed, adding a micro-gripper on top of a miniaturized moving platform dramatically increases the moving mass, decreases the dynamic performances and requires electrical connections through the robot structure, which is particularly difficult to integrate at small scales. Instead, current miniaturized robots were designed as positioning tables that would be used in combination with a deported motionless gripper.

Parallel architectures with a configurable platform provide a solution to add the grasping function to manipulation robots without need of an additional gripper. Indeed, the kinematics of this class of robots offers additional DoFs to the mobile platform that are actuated from the base through the robots' links (*31, 32*). These DoFs are thus part of the kinematic architecture of the robot and do not require any actuators on the platform. The additional DoF of the configurable platform can be used either to generate an additional mobility such as a rotational motion (*33, 34*) or for grasping (*35, 36*). The famous 4-DoFs Quattro Robot from OMRON-ADEPT company (*37*) belongs to this class of robots. Its throughput reaches 200 picks per minute, considering the standard industrial cycle of ADEPT's pick-and-place 25/305/25 mm (i.e. height/distance/height), which makes it one of the fastest industrial robots.

To provide the grasping mobility to the platform, our team proposed a new family of parallel structures based on a folding platform allowing up to 8-DoFs (3 translations + 3 rotations + grasping + in-hand rotation) (*38*).

These manipulators with integrating grasping are composed of spherical joints which cannot be easily miniaturized. Consequently, no miniaturized parallel robot based on soft joints and having a configurable platform has been proposed yet.

In this paper, we present the MiGriBot, a miniaturized parallel robot combining a configurable platform and soft joints (see Fig. 1). The 4-DoFs original kinematic architecture of MiGriBot allows to grasp and manipulate micro-objects (3-translations + grasping). The robotic structure of MiGriBot is composed of a millimeter-scale parallel mechanism actuated with four piezoelectric actuators (see Movie S1). It allows to perform 10 pick-and-place operations per second (considering the Adept cycle 200/600/200 µm) thanks to its integrated grasping capability. The position repeatability of MiGriBot is around 1 µm.

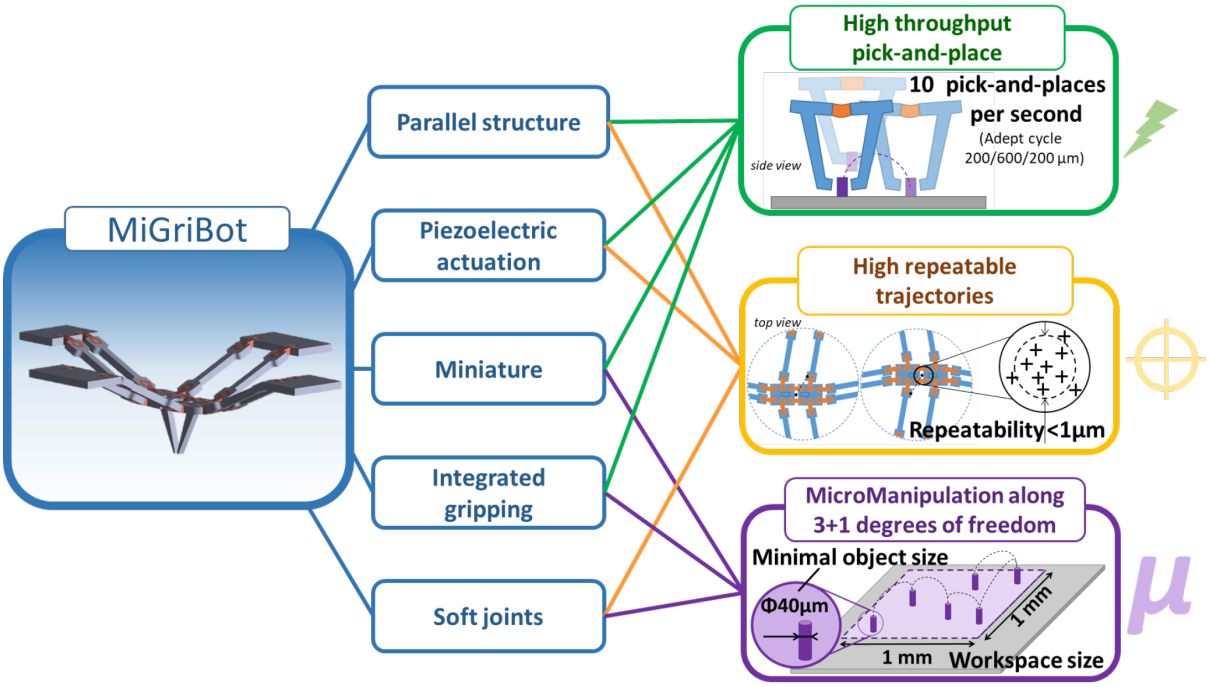

Figure 1: **MiGriBot's main characteritics:** MiGriBot is a miniature robotic manipulator combining a configurable platform and soft joints that performs high throughput trajectories and pick-and-places of micro-objects along a relatively large workspace.

Results

Robotic structure and design

The miniature robotic structure is composed of an actuation system and a parallel mechanism (see Fig. 2.A&B). The actuation system consists of four multilayers piezoelectric bending actuators with embedded position's sensors. Extensions have been attached to the actuator's tips to amplify the output displacements. The stroke of each actuator with its extension is 1 mm ($\pm$ 0.5 mm). Two actuators move along the X-axis and two along the Y-axis. Given the ratio between the length of the actuation system (54.5 mm) and the piezo-bender strokes, the movement of the extensions tips can be considered as translations. The parallel mechanism (see Fig. S1) is composed of silicon rigid links and Polydimethylsiloxane (PDMS) soft joints that act as

spherical joints in the structure (see Fig. 2.C). A pair of same PDMS joints are used to allow the platform to fold. This supplementary DoF is used to grasp micro-objects thanks to the tweezers mounted onto the both part of the configurable platform. Concretely, the configurable platform can be folded with coordinate move of the four limbs (see Fig. 2.D). Thus, the 4-DoFs of the robot, three translations and grasping, are controlled by the four piezo-benders located on the robot's base (see Movie S2). Since no additional active gripper is required, the robot structure is lighter. In addition, no wires (power, signals, etc.) are attached to the robot platform which eliminates unnecessary disturbances from the configurable platform. In conclusion, the MiGri-Bot is highly compact compared to common solutions where the tweezers and its actuators are attached to the rigid platform of a parallel structure. The parallel mechanism has a footprint of 22 mm x 19 mm in his planar configuration. The thickness of the structure is 0.4 mm.

The fabrication of the mechanism consists in molding soft joints into a silicon structure made with cleanroom microfabrication technologies (See Materials and Methods). To prevent separation of the soft joints from the links, we used a specific shape inspired by the design proposed by Vogtmann (*24*) as shown in Fig. 3.F. The robot is thus made in the planar configuration then the tweezers's fingers, whose orientation is orthogonal to the rest of the structure, are assembled on the platform (see Fig. 3.A). Afterward, the basis of the limbs are glued on the actuators' extensions (see Fig. 3.B). The mechanism is then folded from its initial planar configuration (see Fig. 3.C) to reach the home configuration (see Fig. 3.D) which corresponds to the center of the stroke of the actuators.

Finite Element Analyses (FEA) performed on the whole mechanism using Ansys™ have shown that the joints should not experience any damage in the whole range of actuation (see Fig. 3.D&E). In addition, they allow to predict the parallel mechanism behavior from the planar configuration (obtained at the end of the fabrication process) to any pose of the micromanipulator. Last, they have shown that the deformations of the soft joint are very close to a rotation

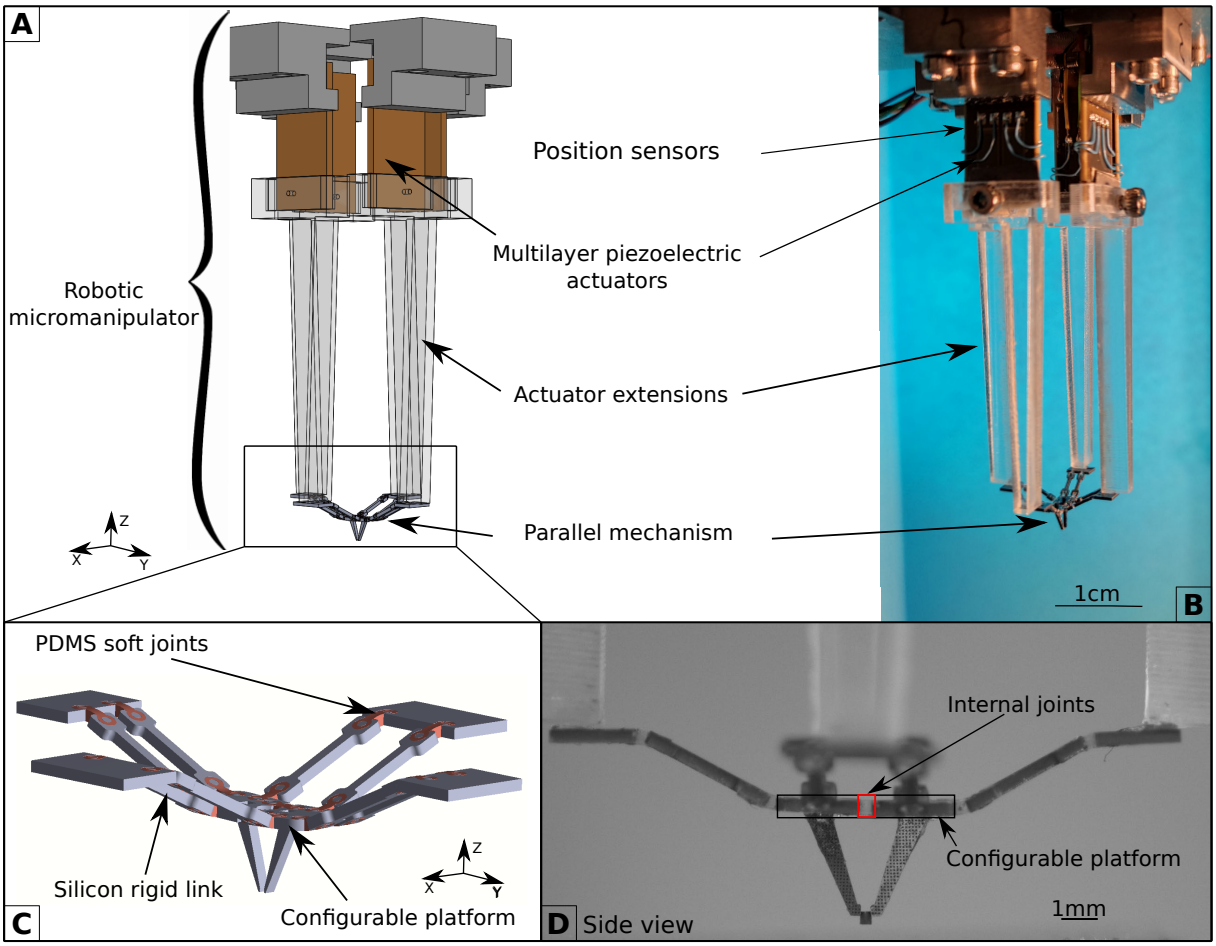

Figure 2: **Presentation of the robotic micromanipulator:** A- Design of the robotic micromanipulator with the actuation system (composed of four multilayers piezoelectric actuators with extensions to amplify their displacements) and the parallel mechanism; B- Picture of the experimental robotic micromanipulator composed of the actuation system and the parallel mechanism; C- Zoom on the parallel mechanism composed of silicon rigid links, soft Polydimethylsiloxane (PDMS) joints and a configurable platform having two internal soft joints; D- Side-focused view on the experimental parallel mechanism gripping a cylinder with a diameter of 350 µm and a height of 400 µm.

around the center of the PDMS part, acting as pseudo-spherical joints.

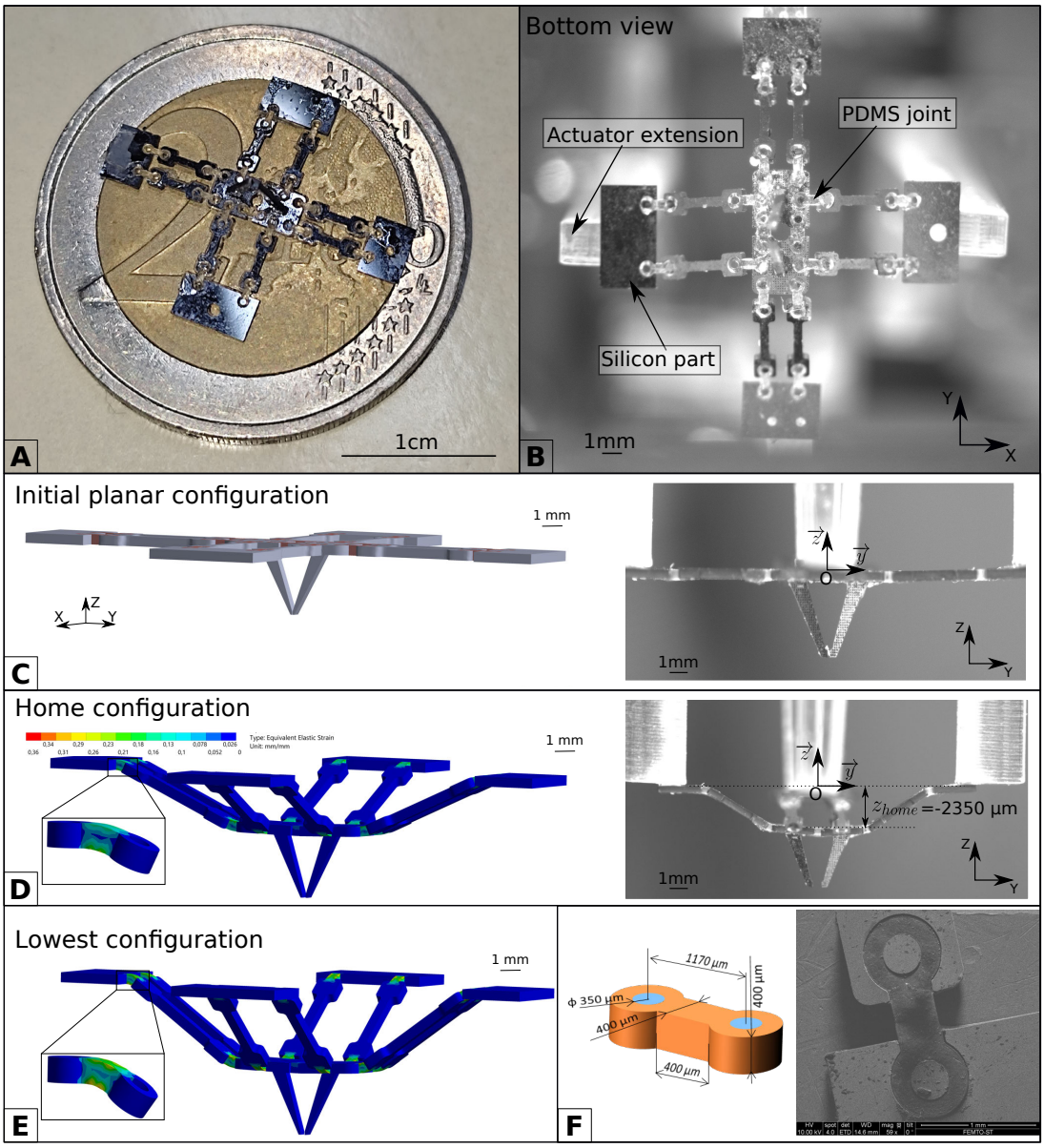

Figure 3: **Microfabrication and mechanical modeling of the parallel mechanism:** A- Parallel mechanism in planar configuration after the assembly of the tweezers; B- Bottom view of the parallel mechanism attached to the actuation system; C- Manipulator in the initial planar configuration at the end of the fabrication process. Please note that the center O of our reference frame $\mathcal{R}_o = (O, \overrightarrow{x}, \overrightarrow{y}, \overrightarrow{z})$ is defined as the center of the top surface of the parallel mechanism in the initial planar configuration; D- Mechanical model and experimental view of the manipulator in the home configuration and zoom on the mechanical constraint in a soft joint; E- Mechanical model when the manipulator is in the lowest configuration; F- Dimension of the PDMS soft joint (before deformation) and example of a Scanning Electron Microscopy (SEM) image of a soft joint.

Robotic micromanipulator performances

This section presents the robot performances in terms of workspace, repeatability and pick-and-place cycle time. The elevation of the home configuration of the manipulator has been chosen in order to maximize the accessible workspace and to avoid singularities. Indeed, the mechanism has at least two singular positions, the planar configuration and the configuration where links are perpendicular to the platform. The workspace corresponding to the chosen elevation has been computed and is illustrated in Fig. 4. A&B. Concretely, the home configuration is defined by the actuators being at the middle of their stroke. The elevation of the home configuration can be adjusted by setting the distances between the actuators. Given the dimensions of the manipulator, the workspace is maximized when the elevation of the home configuration corresponds to $z_{home} = -2.35\,\text{mm}$ (see Fig. 3.D) and when the horizontal position is $x_{home} = y_{home} = 0$ in the reference frame $\mathcal{R}_o$.

Workspace of the micromanipulator

The horizontal workspace (parallel to OXY plane) is maximized at the elevation of the home configuration. Indeed, from this configuration, the entire actuator stroke can be used to move the platform in the horizontal plane and the workspace is consequently a square whose side is the actuator stroke (see Fig. 4.B). The workspace was also analyzed regarding two particular cases: when the tweezers is fully closed and fully opened. As the tweezers actuation is integrated within the structure, we can notice that it has a significant impact on the workspace (see Fig. 4.A). Concretely, in the most conservative point of view, the manipulation workspace is the intersection of both extreme cases making it possible to fully open and close the tweezers everywhere in this workspace (green zone on Fig. 4.A). However, as the top part of the workspace (orange zone on Fig. 4.A) is reachable with closed tweezers, it can be used during the manipulation to transfer grasped objects without releasing them. Due to the structure symmetry of the

robotic manipulator, the same workspace is obtained in OXZ plane and OYZ plane.

Experimental measurements of the workspace have also been performed and show good accordance with the model. Some characteristic points are visible on Fig. 4.C-D-E-F. The slight deviation between experiments and theory visible at the top of the workspace (see Fig. 4.A&F) mainly comes from uncertainties in the assembly process between the parallel mechanism and the actuation system inducing a little asymmetry which can be seen on Fig. 4.F. The tweezers's opening has also been experimentally measured. Fig. 4.G&H present respectively the closed and opened tweezers around the home configuration. It shows that the maximal opening is 540 µm.

Positioning repeatability

Before mounting the robotic structure, a characterization of the positioning repeatability of the actuation system has been made in quasi-static. The measured repeatability, expressed as the standard deviation of the position after 30 repeated visits , is better than 200 nm for positioning the tips of the actuator extensions.

After characterizing the quasi-static performances of the actuation system, the repeatability of the whole robotic micromanipulator was studied (see Fig. S2). Due to the symmetry of the structure, we measured the positioning repeatability only along two axes: the Z-axis and the Y-axis. In the case of the Y-axis, the structure as a very low impact on the positioning as we measured a repeatability better than 600 nm. In the Z-axis, as the structure is deformed and the soft joints are more stressed, we observed a difference in term of repeatability compared to others axes. In this case the obtained repeatability is around 1 µm (see Fig. S2).

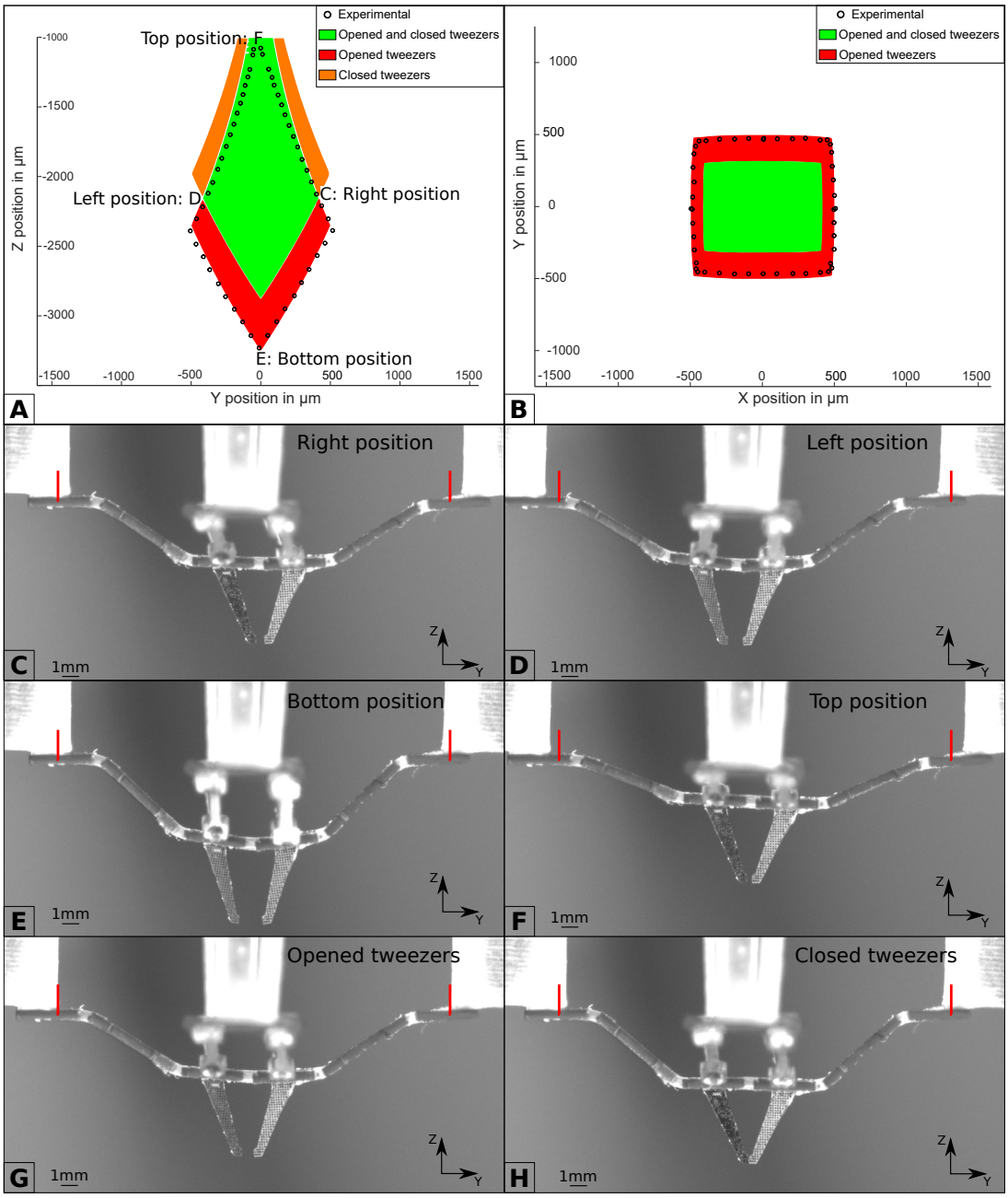

Figure 4: **Workspace of the micromanipulator:** A- Side view (OYZ) of the theoretical and experimental workspaces of the micromanipulator: in green, the workspace accessible whatever the state of the tweezers; in orange, the part accessible only with the closed tweezers; in red, the part accessible only with the opened tweezers; B- Top view (OXY) of the theoretical and experimental workspaces of the micromanipulator; C- Extreme right position along Y axis; D- Extreme left position along Y axis; E- Extreme bottom position along Z axis; F- Extreme top position along Z axis; G- Opened tweezers around home position; H- Closed tweezers at home position.

Lifting capabilities

While manipulating an object, the tweezers should apply a constant force. Since the robotic structure is overconstrained when the gripper is closed, the grasping forces will be distributed over the manipulator structure. Compliance in the manipulator is thus required to perform robotic pick-and-place operations. In fact, in our system, the stiffness of the compliant mechanism is significantly lower than the stiffness of the actuator system which can be considered as rigid. The manipulator compliance is consequently coming from the soft joints. The FEA described in Fig. 3 makes it possible to estimate this compliance for any configurations. For instance, the stiffness of the tweezers in the home configuration is 24.5 Nm^{-1}, enabling a maximum grasping force of 6.6 mN, that is around ten times larger than the parallel mechanism weight.

Given this theoretical grasping force, an experimental validation has been done to evaluate the lifting force. To know the maximum mass that the robot can move from one point to another, several tests have been conducted with objects of increasing masses. The obtained results show that MiGriBot can manipulate objects with masses up to 80 mg but was not able to lift 110 mg (see Movie S7). The ratio between the theoretical grasping force and the highest weight the robot can lift (between 80 mg and 110 mg) corresponds to a friction coefficient between 0.11 and 0.16 which is a plausible friction coefficient range for a Silicon/Stainless steel contact. One can also notice that 80 mg is greater than the mass of the parallel mechanism (65 mg) and sufficiently high when compared to the size of the objects to be manipulated (for example the mass of the cylinder used in the following pick-and-place experiments is 0.07 mg).

High throughput pick-and-place

The main function of the MiGriBot is to manipulate micro-objects at high throughput. The dynamic performances of the micromanipulator and the actuation system have been analyzed and experimentally characterized. Concerning the actuation system, the controllers have been tuned to get a settling time below 10 ms without overshoot and the resulting cut-off frequency is 110 Hz (see Fig. S6) .

To avoid disturbances coming from resonance behavior, the compliant mechanism has been designed to have a first resonant frequency at least 2 times higher than the cut-off frequency of the actuators. The FEA provides the modal analysis of the compliant systems (see Movie S3 and table S1) and shows that the first resonance frequency is 264 Hz in accordance with requirements.

To experimentally validate the capabilities of the designed robotic micromanipulator, we performed the pick-and-place of a silicon cylinder with a diameter of 350 µm and a height of 400 µm at low and high speeds. To facilitate comparisons, the pick-and-place cycle corresponds to a standard Adept cycle of 200/600/200 µm. It is composed of: (i) closing the tweezers to grasp the object from the initial position, (ii) moving it to a target position, (iii) opening the tweezers to release it and (iv) grasping it again to (v) moving it back to the initial position where (vi) opening the tweezers. The whole cycle is described experimentally in Movie S4 with a clear decomposition of each part of the cycle. This cycle has been used to test both low-speed (LS) manipulation and high-speed (HS) manipulation considering a total cycle time of respectively 2 s and 100 ms.

Finally, we realized high-speed (HS) cycles of 100 ms (see Fig. 5.A). Despite the slight dynamic effects visible in the HS-cycle (see Fig. 5.B) inducing small errors on the platform trajectory (see Fig. 5.C), the pick-and-place operations were successful in the HS-cycle (see Movie S6). It shows that the principle, design, and methodologies developed for MiGriBot makes it

possible to reach 10 pick-and-place cycles per second of micro-objects (including forward and backward moves).

A different cycle has been tested at high-speed. This second cycle is the following one: (a) moving from the start position to the picking position, (b) closing the tweezers to grasp the object, (c) moving it to the target position, (d) opening the tweezers to release it and (e) moving back to the start position. The distance between the picking place and the placing position is 600 µm. This cycle is done within 80 ms which can be explained by the fact that there is no need to open and close twice the gripper in comparison with the other cycle. This cycle has been successfully validated using three different objects with 40 µm, 150 µm, and 350 µm thicknesses (see Movie S8).

To show the reproducibility of the handling of the object by the micromanipulator, we perform 10 pick-and-places in a row with the LS-cycle (see Fig. S3 and Movie S5). Given the cut-off frequency of the actuators and the first resonance frequency of the robotic structure, the LS-cycle is considered to be a quasi-static mode.

Performances analyses

Once the capability of MiGriBot to successfully perform the HS-cycle has been validated, we investigate its dynamic limits. To study it, we executed step (ii) of the described cycle at higher speeds without any load in the tweezers and we compared the obtained trajectory to the reference one. As a reminder, step (ii) corresponds to the displacement between the initial position and the target position. In HS-cycle, this *forward trajectory* takes 25 ms. Fig. 6.A presents the side view (in OYZ) of the experimental trajectories for different traveling times. As expected, we can see from this figure that the obtained trajectories get more and more distant from the reference trajectory as the speed increases. It can also be noticed that the three trajectories

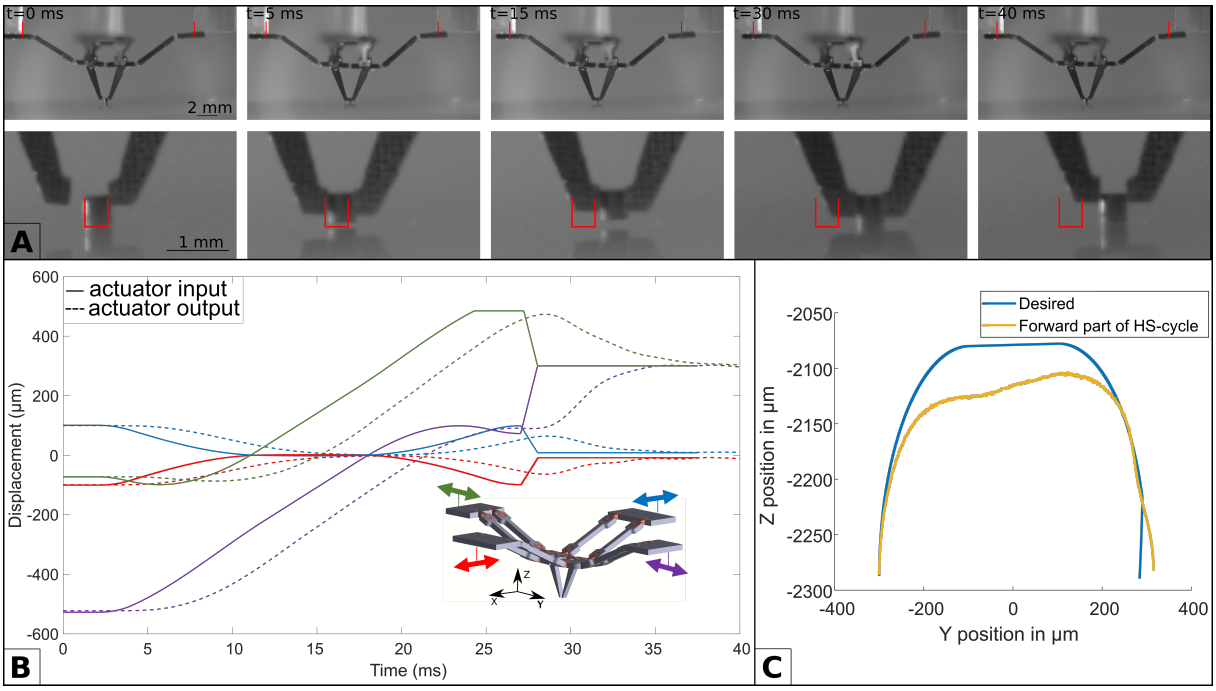

Figure 5: **Experimental demonstrations of pick-and-place operations:** The manipulated object is a 350 µm diameter and 400 µm height silicon cylinder and the result is presented for the forward part of the HS-cycle. A- Motion capture of the manipulator for a pick-and-place HS-cycle. Initial positions of the actuators and the object are represented in red; B- Command vector of each actuator versus the output vector during the forward part of a HS-cycle; C- Trajectory of the end-effectors in the (OYZ) plane for the reference cycle (blue), and HS-cycle (yellow).

(100 ms, 25 ms and 15 ms) are pretty close to each other. However, the 7 ms trajectory is pretty distant from the others which indicates that the impact of inertia and actuation system dynamic significantly increases between 15 ms and 7 ms.

In order to analyze the impact of the robot dynamics on a trajectory which involves more coupling between the several DoFs of the robot, we considered a 600 μm circular trajectory (see Fig. 6.B& C). Considering 10 turns per second (10 Hz), the robotic manipulator is able to follow the reference trajectory. The circles's amplitude decreases as the frequency increases. The -3 dB cut-off frequency of the executed trajectory is about 50 Hz. Since the first resonance frequency of MiGribot is as high as 264 Hz, the resonance mode is not reached. During the different experiments at high-speed, no vibrations of the parallel mechanism were observed which is coherent with the theoretical analysis.

Finally, in order to illustrate the versatility of the MiGriBot, several objects have been handled (see Fig. 7). We demonstrate that the robotic micromanipulator is able to manipulate objects having a thickness from 40 μm to 400 μm. For instance, watch ruby pieces having respectively a cylindrical and parallelipedic shape have been manipulated (see Fig. 7.A&B), a wire with 40 μm diameter has been also successfully grabbed (see Fig. 7.C) and inserted into a 50 μm bore (see Movie S9). Larger objects have also been considered such as watch gears (see Fig. 7.D&E) and the parallel mechanism of another MiGriBot (see Fig. 7.F), which demonstrates that the manipulator is able to hold objects as heavy as its own parallel mechanism.

Discussion

MiGriBot is a new miniature robot able to manipulate objects down to 40 μm in thickness and to perform up to 10 pick-and-place operations per second (considering the Adept cycle 200/600/200 μm). It is based on an original parallel robotic architecture with soft joints and

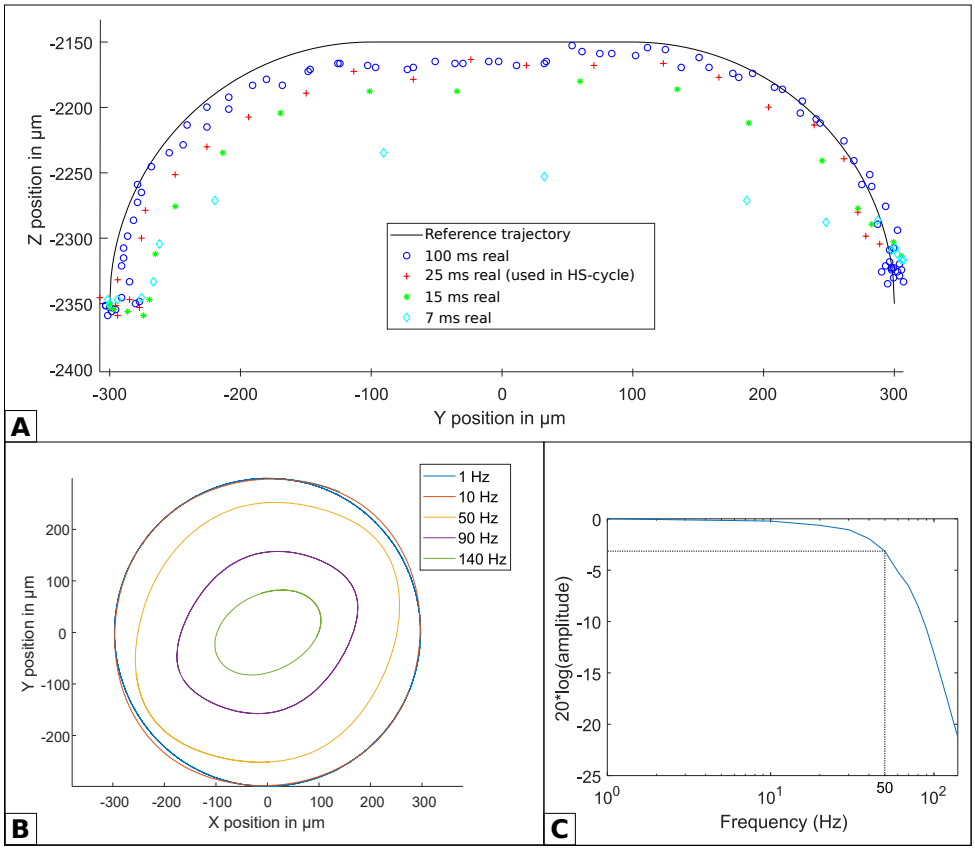

Figure 6: **Experimental high-speed trajectories with no load** A- Side view (OYZ) of the platform trajectory for the *forward trajectory* using different traveling times; B- Top view (OXY) of the configurable platform trajectory for 600 µm diameter circular reference trajectory using different cycle times; C- Bode analysis of the amplitude of the trajectories described in B.

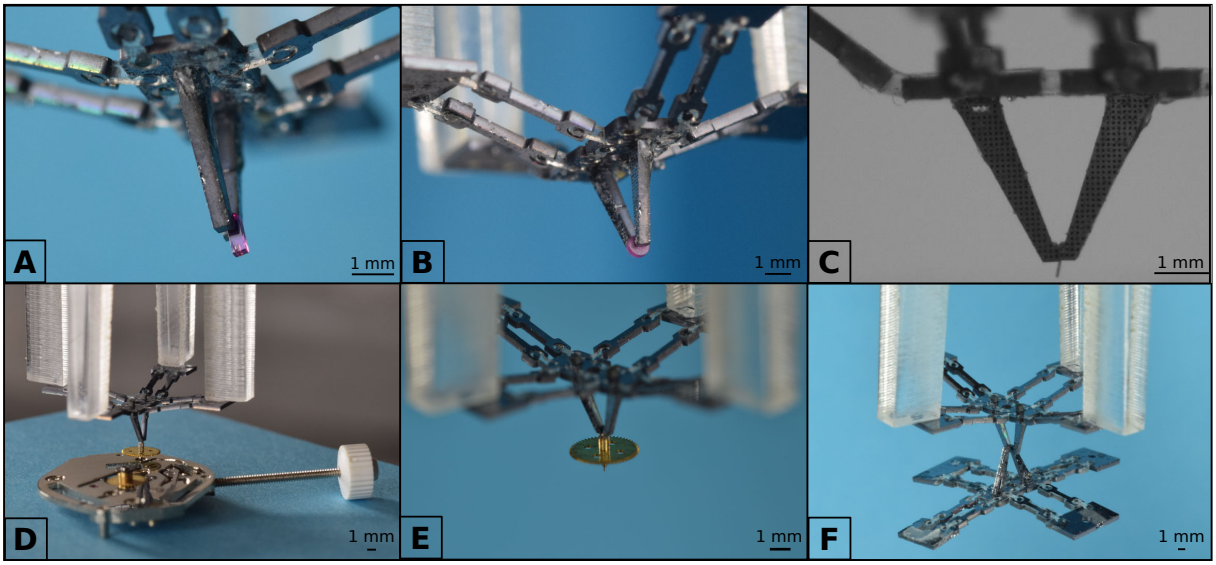

Figure 7: **Manipulation of objects with various shapes and sizes:** A- Grasping of a lever from a Swiss lever escapement with is a parallelepiped ruby with a section of 150 µm by 150 µm and a height of 900 µm; B- Manipulation of a cylindrical ruby with a diameter of 700 µm and a thickness of 200 µm; C- Manipulation of a wire with a diameter of 40 µm ; D- Extraction of a clockwork axis from a watch mechanism, the held diameter is 100 µm; E- Focused view on the grasped clockwork axis; F-Manipulation of another parallel mechanism constituting our robotic micromanipulator. The thickness of the held part is 400 µm.

a configurable platform which is exploited to ensure the grasping capability. All the DoFs of the robot, including grasping, are actuated from the robot's base using instrumented piezoelectric cantilever beams. The compliant mechanism, which consists of silicon links and polymer (PDMS) soft joints, was realized using a dedicated 2-D microfabrication processes and then folded to obtain a 3-D parallel robotic structure. The combination of soft joint, integrated grasping and remote actuation leads to a lightweight structure. Thanks to its low inertia and the closed-loop control of its high bandwidth actuators, MiGriBot is able to perform high-speed pick-and-place operations and to reach a repeatability down to a micron.

Most pick-and-place micro/nano-manipulation cycles reported in the scientific literature range from 6 s to 48 s (*39–42*). Nevertheless, two other works particularly focused on high-speed pick-and-place and were able to reach cycle times of 960 ms (*43*) and 800 ms (*44*), both for 60 µm displacements. The equivalent MiGriBot cycle time reported in this work is 80 ms for a 600 µm displacement. This means that MiGriBot is 10 times faster than the fastest pick-and-place micro-manipulation system reported so far, with a displacement 10 times larger. Furthermore, since the gripper is part of the robot, one can imagine a plenty of MiGriBots working in parallel to simultaneously manipulate millions of micro/nano-objects in a micro-factory (See Fig. S7). This new type of miniaturized parallel robots with integrated grasping opens the way to high-speed micromanipulation and micro-assembly operations in micromanufacturing industries with unprecedented characteristics and performances, namely footprint, repeatability, and throughput.

The positioning repeatability of the MiGriBot depends of the performances of the actuators and the quality of the mechanical structure. The measured repeatability of the actuators extensions tips is five times better than the robot positioning repeatability in Z and three times better than the repeatability on the robot on the Y axis. This can be explained by the coupling and amplification factor of the parallel architecture, combined with the viscoelasticity effect of the soft

joints. Nevertheless, the soft joints allow much larger deformations than hinges in monolithic structures, leading to larger range of motion and larger workspace for comparable structures sizes.

From the design point of view, the performances of the current robot are the result of a trade-off between the size of the whole robot, its workspace and its manipulation throughput. Indeed, the size of current workspace was designed to be relatively comparable to large-scale robotic manipulators (40 μm objects along 1 mm is comparable to 40 mm object along 1 m). To manipulate smaller objects, one can simply reduce the lengths of the actuators extensions, which is one of the main design parameters of the robot. In this case, the robot's workspace would be smaller but its repeatability would be higher. Furthermore, since the robot dynamics is currently limited by the actuators bandwidth (110 Hz) and not by the first resonance frequency of the compliant structure (264 Hz), such as design choice would also increase the robot's throughput. The cut-off frequency of the actuation system is currently two times lower than the first resonance frequency of the parallel mechanism. The goal was to get the maximum bandwidth allowed by the actuators. Nevertheless, reducing the lengths of the actuators extensions would decrease their inertia and increase the bandwidth of the actuation system. To prevent any damage to the parallel mechanism, it should be reduced accordingly to also increase its resonance frequency. Thus, manipulating smaller objects in a smaller workspace would be faster and more precise.

Although, the proposed robot architecture was designed and tested for micro-scale pick-and-place operations, it might also be of interest in nanomanipulation. Indeed, the proposed kinematic architecture has a potential to be more miniaturized since the integrated tweezers need no wiring to be actuated. However, the fabrication of such a robotic manipulator at the nanoscale is still a challenge. Indeed, even if the fabrication of the parallel mechanism is mainly based on very accurate microfabrication techniques that can produce smaller structures, the mechanisms'

assembly on the actuation system and the fingers' assembly on the platform are currently done manually. Using high precision microassembly robots would probably be necessary to be able to assemble more miniature structures and to reduce the assembly uncertainties (*45, 46*).

Materials and Methods

Experimental Set-up

The experimental setup used to control and characterize the proposed kinematic structure is composed of four parts: real-time controller, actuation controller, vision systems and a substrate.

The real-time control is performed using a dSpace RTI1104 card that runs at 2 kHz and delivers four ± 5 V analog signals. The analog signals are then sent to two E-651 drivers that control the four piezoelectric multilayer bending actuators (P-871.112 PICMA® distributed by Physik Instrumente GmbH). The feed-back control is performed thanks to the calibrated strain gauges integrated into the actuators to measure their positions.

Two vision systems are used to characterize the robot's performances and observe the pick-and-place operations. The first vision is composed of two IDS cameras, UI-3280CP-M-GL Rev2 and UI-3040CP-M-GL Rev2, respectively for the side view (OYZ) and the bottom view (OXY). The bottom view is obtained via a 45° mirror and a camera whose axis is placed along the Y axis. This vision setup is used for quasi-static applications and low-speed displacements as these cameras have a standard acquisition frame rate. For the high-speed displacements, we used a second vision system composed of a high-speed camera Phantom Miro M310 and an external LED lighting. The main challenges were to have a good image contrast, a large depth of focus and a low µm to pixel ratio for the post-treatment of the images.

The last part of the experimental setup is the substrate and the manipulated object on it. In

most of the experiments, the manipulated object was a cylinder with a diameter of 350 µm and a height of 400 µm made of silicon. Because of the size of the object and the adhesion forces that predominate at this scale, the release of the object can be problematic. To avoid the release issues, a Gel-Pak® -4- film has been used as a substrate. More details about the experimental setup can be found in the supplementary material as well as a block diagram (see Fig. S4) and pictures (see Fig. S5).

Modeling and design of the robot

The robot and the experimental setup have been designed using Solidworks™ 2018. The computer used for the modeling and the simulation is a PC equipped with an Intel Core i5-10400H CPU running at 2.60 GHz and 16 Go of RAM.

Finite Element Analyses have been done using Ansys™ 2019. As soft joints experience large deformations, a large deformation solver has been used which induces a high computational time. To reduce computational time for the different analyses, the first deformation which is the displacement from the planar initial configuration to the home configuration (see Fig. 3) of the analysis is done only once. Other simulations are computed from this home configuration state, which reduces the running time of a simulation. This home configuration is also used as the reference position for the modal analysis of the structure.

The finite element model has been used to simulate the forward kinematics of the robot and to carry out the modal analysis. However, to control the robot in real time, the finite element method is too slow. So, we established in a second time the inverse kinematics of the robot by solving the closure equations and considering that joints are perfect spherical ones. Indeed, the soft joints have been designed to act as spherical joints. This design have been introduced and validated previously with experiments in (*28*) and comparisons between the finite element model and the kinematic one have shown that the position errors do not exceed 5% of the

workspace length.

During the pick-and-place cycles, the trajectory generation has been done in real-time with trapezoidal speed profiles and using the inverse kinematics of the parallel structure.

Parallel mechanism fabrication

As the parallel mechanism is composed of PDMS joints and rigid silicon parts, a specific micro-fabrication process has been developed and published in (*28*). PDMS is particularly well suited for making micro soft joints. It is a fluid polymer which can be easily be molded in small holes (400 µm in this case). In addition, after polymerisation PDMS is very soft so its bending does not requires too high forces/moments from the actuators. This was required to get a kinematic behavior close to spherical joints.

The first step of the process consists of a deposition of a 2 µm layer of aluminum on the back-side of a silicon wafer which will be used as a stop layer of etching. Secondly, a spin coating of a 7 µm layer of photoresist is performed on the front side. The structure of the manipulator and tweezers are then obtained by the Deep Reaction Ion Etching (DRIE) technique through the silicon wafer. Before molding the PDMS, a spray coating of photoresist is performed on the front side of the wafer to create the specific areas in which the PDMS will be placed. After this step, a wafer support is bonded with vacuum-compatible oil to support the etched wafer and the aluminum membrane. Then, the etched areas are filled with PDMS. Finally, the support wafer, the remaining PDMS, and the aluminum membrane are released in order to obtain the parallel mechanism and the tweezers. To obtain the final manipulator mechanism, two fingers of the tweezers are manually assembled on each on a part of the configurable platform (see Fig. 3.A).

After this step, the parallel mechanism is ready to be glued onto the actuators' extensions (see Fig. 3.B). The main issues at this stage are (i) maintaining the planar configuration during the assembly and (ii) the alignment of the silicon links with the actuators axes. A specific

mechanical support was designed and used during the gluing operation to help for the appropriate positioning of the mechanism. Once the mechanism is attached to the actuators, it has to move away from the planar configuration, which is singular, to get to the home configuration (see Fig. 3.C). Linear positioning stages are thus used to place the actuators at their reference positions. If the gravity force is not sufficient to displace the parallel mechanism to the right position, a little force along the Z-axis is applied on the platform to reach the home configuration (see Fig. 3.D). A known issue of using PDMS with silicon is that both material do not stick well together. In other words, the adherence between PDMS soft joints and silicon part is low. To ensure the stability of the joints, puzzle shapes are used with small cylinder inside the tenon to prevent dislocation. Several robots have been realized with success and no breakage have been notice even after high-speed displacements made during the experimental campaign showing that those links are reliable.

Supplementary materials

Text

Table S1. Modal analysis of the parallel mechanism.

Fig. S1. Design and mechanical properties of the parallel mechanism.

Fig. S2. Experimental repeatability of the robotic structure.

Fig. S3. Analysis of the forward part of the LS-cycle (Low Speed - 2 s) pick-and-place cycle.

Fig. S4. Block diagram of the control architecture of MiGriBot.

Fig. S5. Experimental setup.

Fig. S6. Dynamical analysis of the actuation system.

Fig. S7. Illustration of a parallel micro-assembly line using several MiGriBots.

Movie S1. General principle and structure of MiGriBot.

Movie S2. The 4 degrees of freedom of MiGriBot.

Movie S3. Modal analysis of MiGriBot.

Movie S4. MiGriBot: Quasi-static pick-and-place sequence.

Movie S5. MiGriBot: 10 experimental pick-and-place operations of a micro-object using low-speed cycle (2 s).

Movie S6. MiGriBot: Experimental pick-and-place operation of a micro-object with high-speed cycle (100 ms).

Movie S7. Maximal weight carried by MiGriBot.

Movie S8. General pick-and-place operation of micro-objects with high-speed cycle (80 ms).

Movie S9. Manipulation and insertion into a 50 µm bore of a 40 µm diameter pin.

References

1. H. McClintock, F. Z. Temel, N. Doshi, J.-s. Koh, R. J. Wood, The millidelta: A high-bandwidth, high-precision, millimeter-scale delta robot, *Science Robotics* **3** (2018).

2. J.-P. Merlet, *Parallel robots*, vol. 128 (Springer Science & Business Media, 2006).

3. R. Clavel, A fast robot with parallel geometry, *Proc. of the Int. Symposium on Industrial Robots* (1988), pp. 91–100.

4. F. Pierrot, C. Reynaud, A. Fournier, Delta: a simple and efficient parallel robot, *Robotica* **8**, 105–109 (1990).

5. M. Gauthier, C. Clevy, P. Kallio, D. Heriban, Industrial tools for micromanipulation, *Micro- and Nanomanipulation Tools* (Wiley, 2015), pp. 369–392.

6. A. Ghosh, B. Corves, *Introduction to micromechanisms and microactuators* (Springer, 2015).

7. C. Shi, *et al.*, Recent advances in nanorobotic manipulation inside scanning electron microscopes, *Microsystems & Nanoengineering* **2**, 16024 (2016).

8. M. Richard, R. Clavel, Concept of modular flexure-based mechanisms for ultra-high precision robot design, *Mechanical Sciences* **2**, 99–107 (2011).

9. Y. Bellouard, *Microrobotics: methods and applications* (CRC Press, 2019).

10. D. Brouwer, B. de Jong, H. Soemers, Design and modeling of a six DOFs MEMS-based precision manipulator, *Precision Engineering* **34**, 307–319 (2010).

11. R. Zhang, A. Sherehiy, D. Wei, D. O. Popa, Design and characterization of solid articulated four axes microrobot for microfactory applications, *Journal of Micro-Bio Robotics* **15**, 119–131 (2019).

12. S. H. Yang, Y.-S. Kim, J.-M. Yoo, N. G. Dagalakis, Microelectromechanical systems based stewart platform with sub-nano resolution, *Applied Physics Letters* **101**, 061909 (2012).

13. C. E. Bryson, D. C. Rucker, Toward parallel continuum manipulators, *2014 IEEE International Conference on Robotics and Automation (ICRA)* (IEEE, 2014), pp. 778–785.

14. C. B. Black, J. Till, D. C. Rucker, Parallel continuum robots: Modeling, analysis, and actuation-based force sensing, *IEEE Transactions on Robotics* **34**, 29–47 (2017).

15. B. Mauze, *et al.*, Nanometer Precision with a Planar Parallel Continuum Robot, *IEEE Robotics and Automation Letters* **5**, 3806–3813 (2020).

16. F. Largilliere, *et al.*, Real-time control of soft-robots using asynchronous finite element modeling, *2015 IEEE International Conference on Robotics and Automation (ICRA)* (IEEE, 2015), pp. 2550–2555.

17. M. Gazzola, L. H. Dudte, A. G. McCormick, L. Mahadevan, Forward and inverse problems in the mechanics of soft filaments, *Royal Society Open Science* **5** (2018).

18. J. Till, V. Aloi, C. Rucker, Real-time dynamics of soft and continuum robots based on Cosserat rod models, *International Journal of Robotics Research* **38**, 723–746 (2019).

19. B. Mauzé, G. J. Laurent, R. Dahmouche, C. Clévy, Micrometer Positioning Accuracy With a Planar Parallel Continuum Robot, *Frontiers in Robotics and AI* **8**, 1–13 (2021).

20. J. E. Correa, J. Toombs, N. Toombs, P. M. Ferreira, Laminated micro-machine: Design and fabrication of a flexure-based delta robot, *Journal of Manufacturing Processes* **24**, 370–375 (2016).

21. H. Suzuki, R. J. Wood, Origami-inspired miniature manipulator for teleoperated microsurgery, *Nature Machine Intelligence* **2**, 437–446 (2020).

22. S. Mintchev, M. Salerno, A. Cherpillod, S. Scaduto, J. Paik, A portable three-degrees-of-freedom force feedback origami robot for human–robot interactions, *Nature Machine Intelligence* **1**, 584–593 (2019).

23. M. Z. Miskin, *et al.*, Electronically integrated, mass-manufactured, microscopic robots, *Nature* **584**, 557–561 (2020).

24. D. E. Vogtmann, S. K. Gupta, S. Bergbreiter, Characterization and modeling of elastomeric joints in miniature compliant mechanisms, *Journal of Mechanisms and Robotics* **5**, 041017 (2013).

25. A. DeMario, J. Zhao, Development and analysis of a three-dimensional printed miniature walking robot with soft joints and links, *Journal of Mechanisms and Robotics* **10** (2018).

26. J. Zhang, *et al.*, Voxelated three-dimensional miniature magnetic soft machines via multimaterial heterogeneous assembly, *Science Robotics* **6** (2021).

27. D. Martella, S. Nocentini, D. Nuzhdin, C. Parmeggiani, D. S. Wiersma, Photonic Microhand with Autonomous Action, *Advanced Materials*, **29**, pp. 1704047 (2017).

28. W. Haouas, R. Dahmouche, J. Agnus, N. L. Fort-Piat, G. J. Laurent, New integrated silicon-PDMS process for compliant micro-mechanisms, *Journal of Micromechanics and Microengineering* **27** (2017).

29. Z. Zhang, X. Wang, J. Liu, C. Dai, Y. Sun, Robotic micromanipulation: Fundamentals and applications, *Annual Review of Control, Robotics, and Autonomous Systems* **2**, 181-203 (2019).

30. R. Li, H. Qiao, A survey of methods and strategies for high-precision robotic grasping and assembly tasks—some new trends, *IEEE/ASME Transactions on Mechatronics* **24**, 2718-2732 (2019).

31. P. Lambert, J. L. Herder, Parallel robots with configurable platforms: Fundamental aspects of a new class of robotic architectures, *Proceedings of the Institution of Mechanical Engineers, Part C: Journal of Mechanical Engineering Science* **230**, 463–472 (2016).

32. P. Lambert, J. L. Herder, A 7-dof redundantly actuated parallel haptic device combining 6-dof manipulation and 1-dof grasping, *Mechanism and Machine Theory* **134**, 349-364 (2019).

33. F. Pierrot, O. Company, H4: a new family of 4-DOF parallel robots, *1999 IEEE/ASME International Conference on Advanced Intelligent Mechatronics (Cat. No.99TH8399)* (1999).

34. F. Pierrot, O. Company, F. Marquet, H4: A High Speed 4dof Parallel Robot. Synthesis, Modeling and Control Issues, *IEEE Transactions on Robotics and Automation* **19**, pp. 411-420 (2003).

35. B.-J. Yi, *et al.*, Design of a parallel-type gripper mechanism, *The International Journal of Robotics Research* **21**, 661–676 (2002).

36. V. Babin, C. Gosselin, Mechanisms for robotic grasping and manipulation, *Annual Review of Control, Robotics, and Autonomous Systems* **4** (2021).

37. F. Pierrot, V. Nabat, O. Company, S. Krut, P. Poignet, Optimal design of a 4-dof parallel manipulator: From academia to industry, *IEEE Transactions on Robotics* **25**, 213-224 (2009).

38. W. Haouas, R. Dahmouche, N. Le Fort-Piat, G. J. Laurent, A new seven degrees-of-freedom parallel robot with a foldable platform, *Journal of Mechanisms and Robotics* **10** (2018).

39. Y. Zhang, B.K. Chen, X. Liu, Y. Sun, Autonomous robotic pick-and-place of microobjects, *IEEE Transactions on Robotics* **26**, pp. 200-207 (2009)

40. R.K. Jain, S. Majumder, B. Ghosh, S. Saha, Design and manufacturing of mobile micro manipulation system with a compliant piezoelectric actuator based micro gripper , *Journal of Manufacturing Systems* **35**, pp. 76-91 (2015).

41. M. Lofroth, E. Avci, Development of a Novel Modular Compliant Gripper for Manipulation of Micro Objects , *Micromachines* **10**, pp. 313 (2019).

42. H. Xie, S. Régnier, Three-dimensional automated micromanipulation using a nanotip gripper with multi-feedback, *Journal of Micromechanics and Microengineering* **19**, pp. 075009 (2009).

43. E. Avci, K. Ohara, C.N. Nguyen, C. Theeravithayangkura, M. Kojima, T. Tanikawa, T. Arai, High-speed automated manipulation of microobjects using a two-fingered microhand, *IEEE Transactions on Industrial Electronics* **62**, pp. 1070-1079 (2014).

44. E. Kim, M. Kojima, Y. Mae, T. Arai, High-speed manipulation of microobjects using an automated two-fingered microhand for 3d microassembly, *Micromachines* **11**, pp. 534 (2020).

45. A. Benouhiba, L. Wurtz, J.-Y. Rauch, J. Agnus, K. Rabenorosoa, C. Clevy, NanoRobotic Structures with Embedded Actuation via Ion Induced Folding, *Advanced Materials* **33**, pp.2103371 (2021).

46. J.-Y. Rauch, O. Lehmann, P. Rougeot, J. Abadie, J. Agnus, M. A. Suarez, Smallest microhouse in the world, assembled on the facet of an optical fiber by origami and welded in the microRobotex nanofactory , *Journal of Vacuum Science and Technology A, American Vacuum Society* **36**, pp.41601 (2018).

Acknowledgments

We thank J. Agnus and D. Belharet for their technological assistance during the cleanroom fabrication. **Funding:** This work was supported by the Grand Besançon Métropole, the French ANR project MiniSoRo (ANR-19-CE10-0004), ROBOTEX network (ANR-21-ESRE-0015), and by EUR EIPHI program (ANR-17-EURE-0002). This work was carried out in part within

the french RENATECH network and its FEMTO-ST technological facility. **Author contributions:** R.D. proposed the original idea and the robot architecture. W.H., G.J.L., R.D. initiated the project. M.L., W.H. fabricated the robot. M.L. performed the numerical simulations and the experimental tests, managed the statistical analysis of the data and write the first draft of the paper. G.J.L., W.H. assisted M.L. in the modeling. All authors contributed to the methodology and in the manuscript preparation. M.L., G.J.L., M.G. contributed to the data presentation and visualization. G.J.L., M.G., R.D., managed the research project including providing resources and funding acquisition. **Competing interests:** The authors declare that they have no competing interests. **Data and materials availability:** All data needed to evaluate the conclusions in the paper are present in the paper and/or the Supplementary Materials.

Supplementary Materials

Design and mechanical properties of the parallel mechanism

The design of the parallel mechanism is described in Fig. S1. The mechanism is based on the high difference between the Young modulus of the PDMS (1.4 MPa) and the silicon (160 GPa) making it possible to concentrate the deformation in the PDMS joints

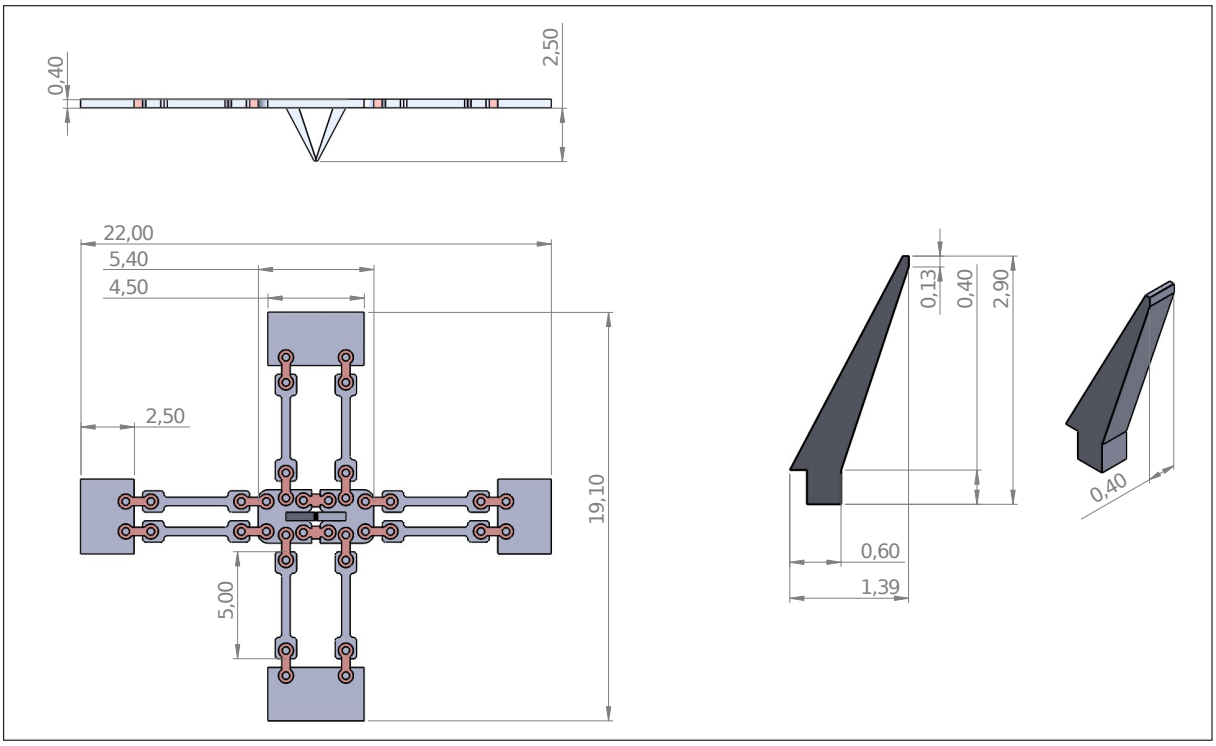

Fig. S1. Design of the parallel mechanism. Dimensions are in mm.

To ensure that the actuator forces (the blocking force is 2 N) were sufficient to deform the structure through their extensions, we carried out some finite element simulations. The result is that to generate the folding for the structure, a force of only 6 mN is needed. This result shows that the chosen actuators are suitable for the application but also reveals another advantages of using soft joints.

Modal analysis of the parallel mechanism

The modal analysis of the parallel mechanism has been performed using Ansys™ software. The results are available in table S1. The different modes can be further appreciated in Movie S3.

Mode	1	2	3	4	5	6
Frequency (Hz)	264.51	392.76	455.52	639.05	715.49	1028.6

Table S1. Modal analysis of the parallel mechanism. Frequencies are obtained by performing a modal analysis around the home configuration of the manipulator with a FEM model

Measurement protocol of the positioning repeatability

To determine the ability of the robotic micromanipulator to manipulate an object with good repeatability, several experiments have been done (see Fig. S2). Firstly, the study has been focused on the actuation system without the parallel mechanism. Secondly, the whole platform has been characterized. The experimental protocol remains basically the same in both cases. The experiment was made using 30 round trips between four positions in the workspace: point A (z=-2.05 mm and y=0 mm), point B (z=-2.35 mm and y=0 mm), point C (z=-2.35 mm and y=-0.25 mm) and point D (z=-2.35 mm and y=0.25 mm). It can be notice that in the Y direction, the distance between the two points is 500 µm and in the Z direction this distance is 300 µm. Thus, they cover 50% of the workspace width and are relevant for the desired pick-and-place application (see Fig. S2.E).

The repeatability is then expressed as the standard deviation of the 30 measures. For the actuation system, a fiducial marker was glued at the tip of the actuator extension and the position measurement was performed using a holographic microscope. Following this protocol, the repeatability of the actuation system is measured at 200 nm, a value close to the in-plane resolution of the microscope. Concretely, it means that the repeatability is equal to or better

than 200 nm. Concerning the characterization of the whole robotic manipulator, we have considered two cases: (i) the movements along X and Y and (ii) the movement along Z. Indeed, both types of movement do not have the same performances. The movements in the OXY plane have better repeatability than along Z where the compliant mechanism is more deformed. To be able to measure with a high resolution the position of the platform, a periodic pattern has been engraved on the gripper fingers and a digital image correlation was used (imregcorr function from Matlab™). Once again, the measurement could be limited by the resolution of the method. The results show a resolution better than 600 nm in OXY plane and around 1 µm along Z.

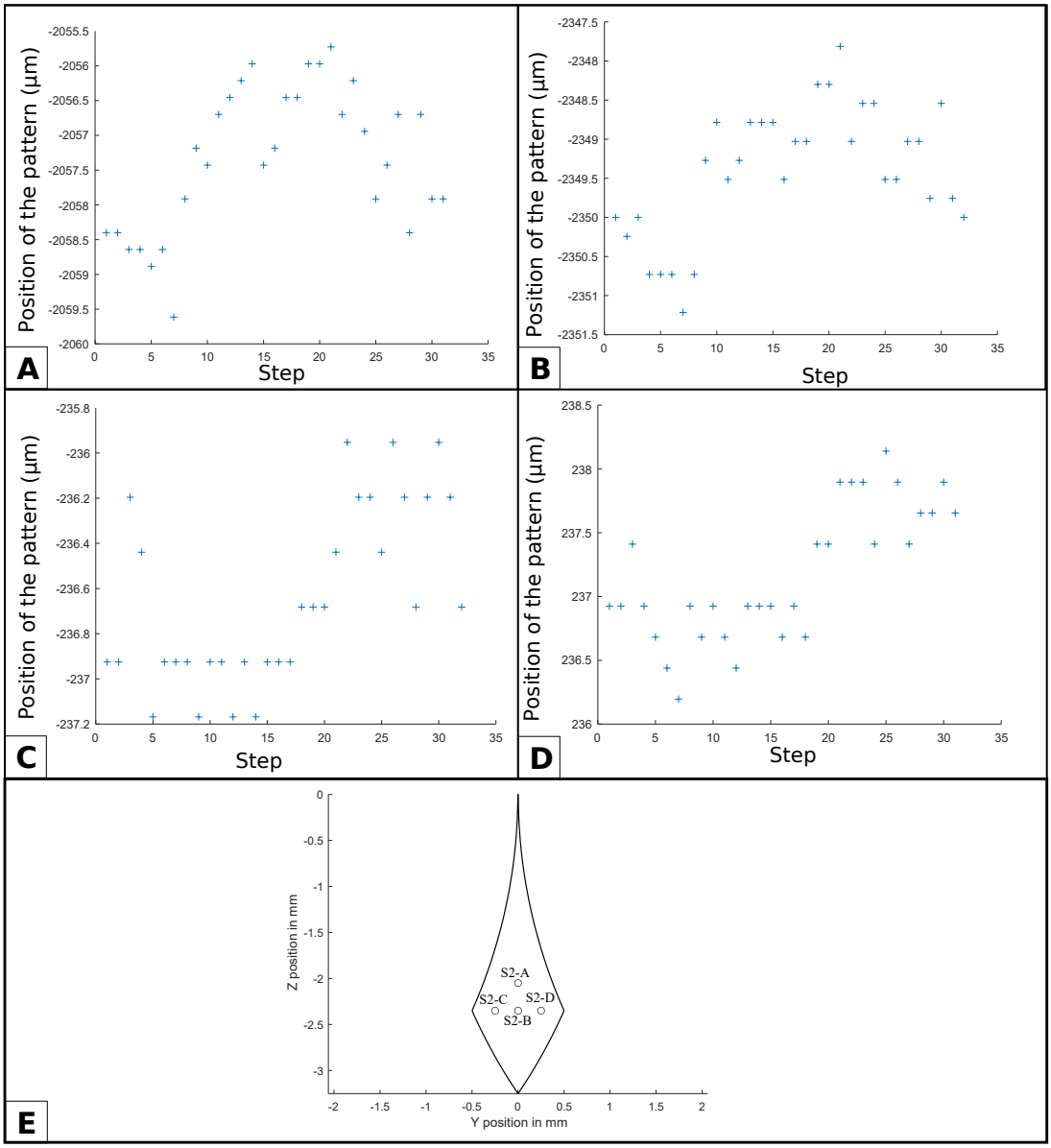

Fig. S2. Experimental repeatability of the robotic structure. A- Repeatability in the Z direction at the highest point of the study (STD= 1.038 µm); B- Repeatability in the Z direction at the lowest point of the study (STD= 0.8395 µm); C- Repeatability in the Y direction at first point of the study (STD= 0.3910 µm); D- Repeatability in the Y direction at the second point of the study (STD= 0.5267 µm); E- Positions of the tested points for the repeatability experiments .

Analysis of the forward part of the pick-and-place LS-cycle

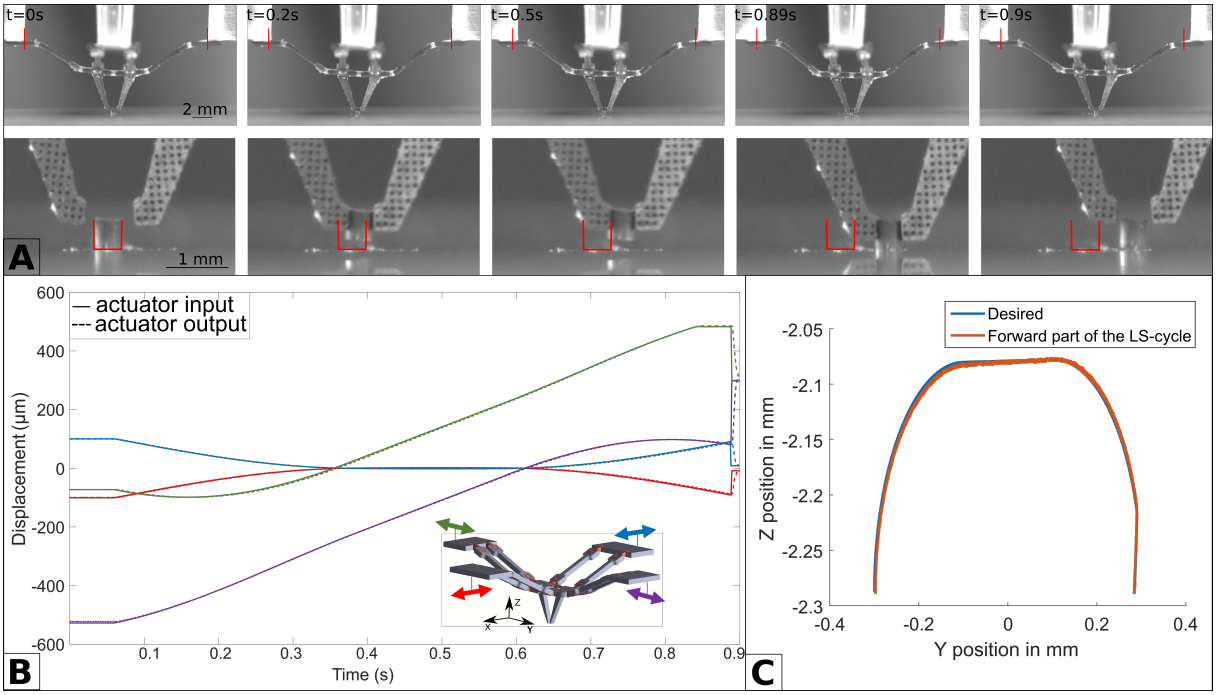

Fig. S3. Analysis of the forward part of the LS-cycle (Low Speed - 2 s) pick-and-place cycle. The manipulated object is a 350 µm diameter and 400 µm height silicon cylinder and the result is presented for the forward part of the LS-cycle which can be considered as quasi-static. A- Motion capture of the first 0.9 s of the LS-cycle where the manipulator graps and moves the object form the initial position to the final one. Initial positions of the actuators and the object are represented in red; B- Command vector of each actuator versus the output vector during the first 0.9 s of the LS-cycle; C- Trajectory of the end-effectors in the (OYZ) plan for the reference cycle (blue), during the first 0.9 s of the LS-cycle (red).

Control Architecture of MiGriBot

The control architecture of MiGriBot can be decomposed into three main parts: the dSpace real-time system, the four actuator controllers and MiGriBot. The first part (in red in Fig. S4) is composed of a dSpace real-time controller programmed with Matlab/Simulink which integrates the trajectory generation. The second part (in blue in Fig. S4) is the controller from Physik Instrumente GmbH of the actuators with the closed-loop on the position sensors of each actuators. Those controllers have been tuned following the datasheet in order to obtain the good behavior with the extension. The third part (in green in Fig. S4) is MiGriBot composed of the parallel mechanism and the actuation system (4 actuators and their extensions). The entry of the control system is the target position of MiGribot. Then the dSpace real-time system makes the trajectory generation between the target position and the current position following trapezoidal velocity profiles. Then the Cartesian positions are expressed in the joint space thanks to the inverse kinematic model which is also implemented in the dSpace real-time system.

The joint position vector is sent to the actuator controller in order to actuate each piezo-electric actuator with the calculated displacements. A position sensor gives a feedback on the actuator position and a control loop is then used to control precisely the position of the actuator.

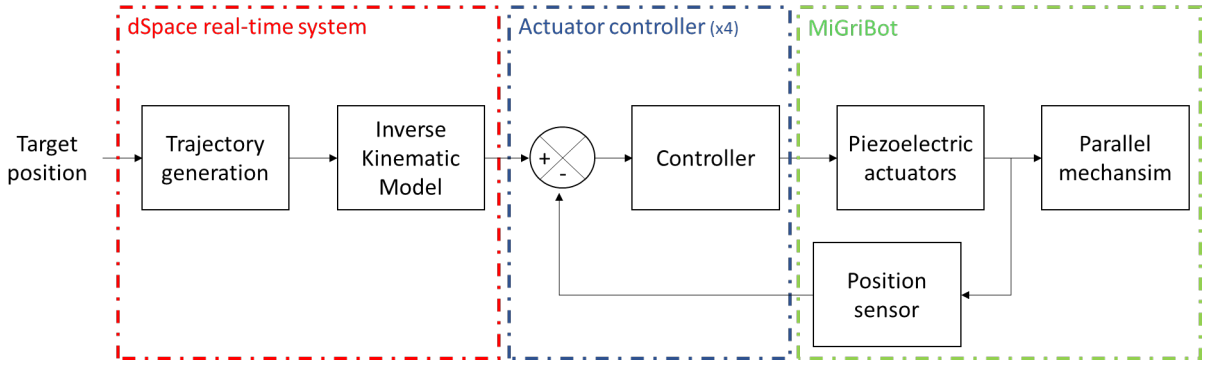

Fig. S4. Block diagram of the control architecture of MiGriBot. Control architecture of MiGriBot from the target position to the displacement and deformation of the parallel mechanism. It is composed of three main parts, the dSpace real-time system, the actuator controller and MiGriBot.

Experimental setup

Fig. S5 gives more details about the experimental setup and the working environment of MiGriBot. Fig. S5.A is highly related to the block diagram described in Fig.S4 as the entire control chain is visible with the supervision computer, the dSpace real-time system, the four actuator controllers and the working station integrating the MiGriBot. Fig. S5.B gives more details about the positioning of the cameras in order to get the side and bottom views of the manipulator. For the high-speed displacements, the conventional side view camera was replaced by the high-speed camera Phantom Miro M310 and an external LED lighting was added. Concerning the bottom view, a 45° mirror has been placed under the parallel mechanism as shown in the Fig. S5.C. The last part of the experimental setup is the manipulation substrate located between the parallel mechanism and the mirror (see Fig. S5.D).

The measurements of the finger positions for the trajectories analysis and for the positioning repeatability evaluation have been done using image correlation in post processing. An orthographic projection model has been used since the macro objectives have very long focal lengths. The scale was measured thanks to the dots grids visible of the fingers and with the known lengths of the links of the robots for bottom views. All the displacements were measured

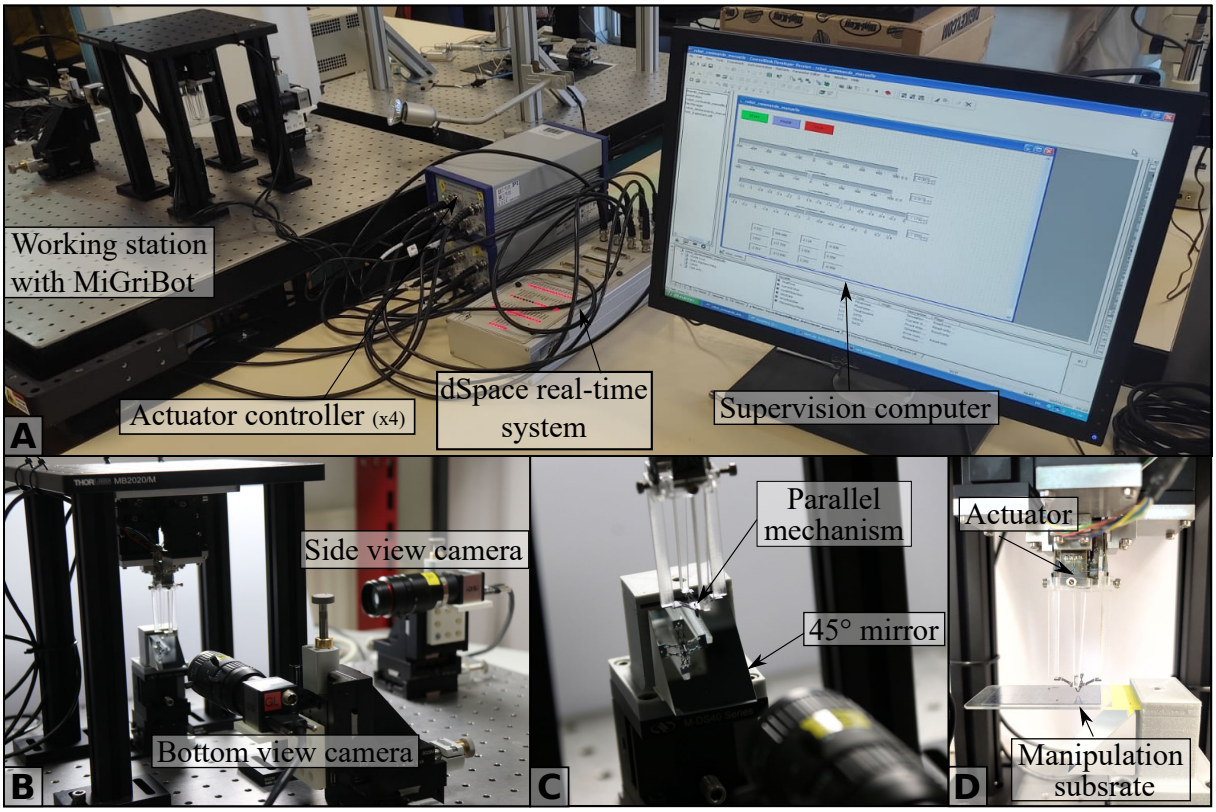

Fig. S5. Experimental setup. A- Whole experimental setup with the supervision computer, the dSpace real-time system, the four actuator controllers and the working station integrating the MiGriBot; B- Position of the two cameras used for the side and bottom views. Note that the side view camera was replaced by the high-speed camera when needed; C- Details about the generation of the bottom view of the parallel mechanism with a 45° mirror; D- MiGriBot and the manipulation substrate used for the experimentation

through template matching.

All the experiments described in this paper have been done with the same MiGriBot for more than ten months. This long time of use shows that the soft joints properties and behaviors remain stable in time. Another aspect is the durability of the robot during continuous operations. In this respect, the robot was able to perform Z displacements at low speed during two hours straight without any damage.

Dynamic analysis of the actuation system

To analyze the dynamic performances of MiGriBot a key information is the bandwidth of the actuation system. Indeed, this information will give more details about the dynamic limitation of the current version of MiGriBot. Two main limitations can be spotted: the actuation system dynamic and the inertia of the structure. The Fig. S6 gives the bode diagram in amplitude of the actuation system and its step response. Fig. S6.A shows that the cut-off frequency at -3 dB of the actuation system is around 110 Hz. The Fig. S6.B gives the response of each actuation unit to a step of 200 µm. The four actuation units have the settling time which lies between 7.7 ms and 9.3 ms to reach the set point. This dynamic analysis confirms that with the current actuation it is not possible to perform faster pick-and-place applications. To improve the dynamic performances of the robot, new actuators have to be found.

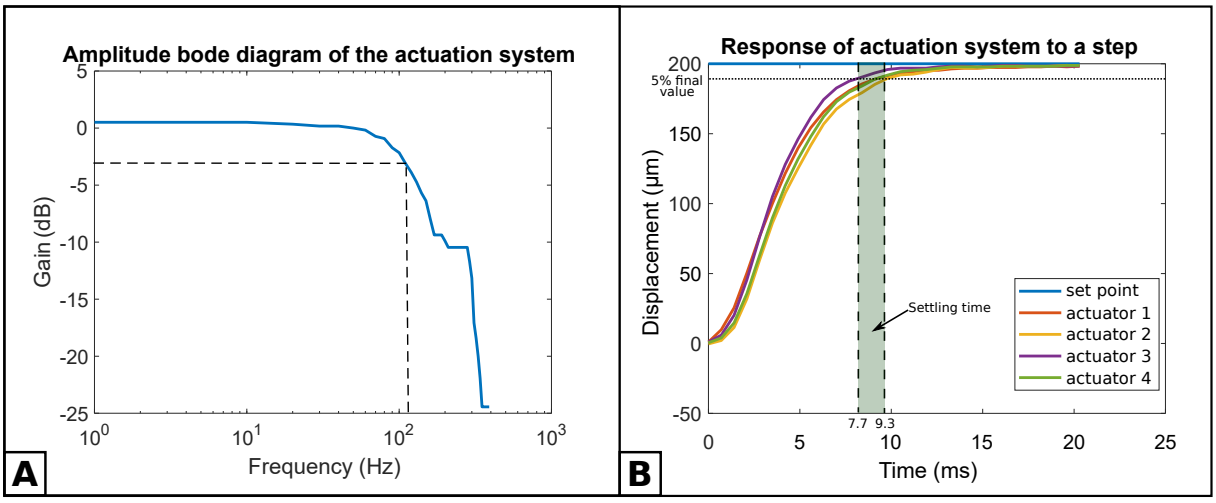

Fig. S6. Dynamical analysis of the actuation system. A- Bode diagram in amplitude of the actuation unit in closed-loop; B- Response of actuation units to a step of 200 µm in closed-loop. The settling time for this displacement lies between 7.7 ms and 9.3 ms depending on the actuation unit.

Parallel micromanipulation using several MiGriBots.

Having a compact microgripper with its own translation capability enables to place several MiGribots (typ. 10) up to a table working in parallel. It will enable to increase the global throughput by one order of magnitude: reaching typically 100 pick-and-place per second performed by 10 MiGriBots. A typical example of application benchmark is represented in Fig. S7. In this example, micro-objects are initially fabricated onto a wafer using microfabrication techniques. The wafer is placed on a high-speed 2D positioning table in order to place the objects close to each MicroGriBot. The object are grasped on the wafer and placed on some microsystems or micropalette using the 10 MiGriBots working in parallel.

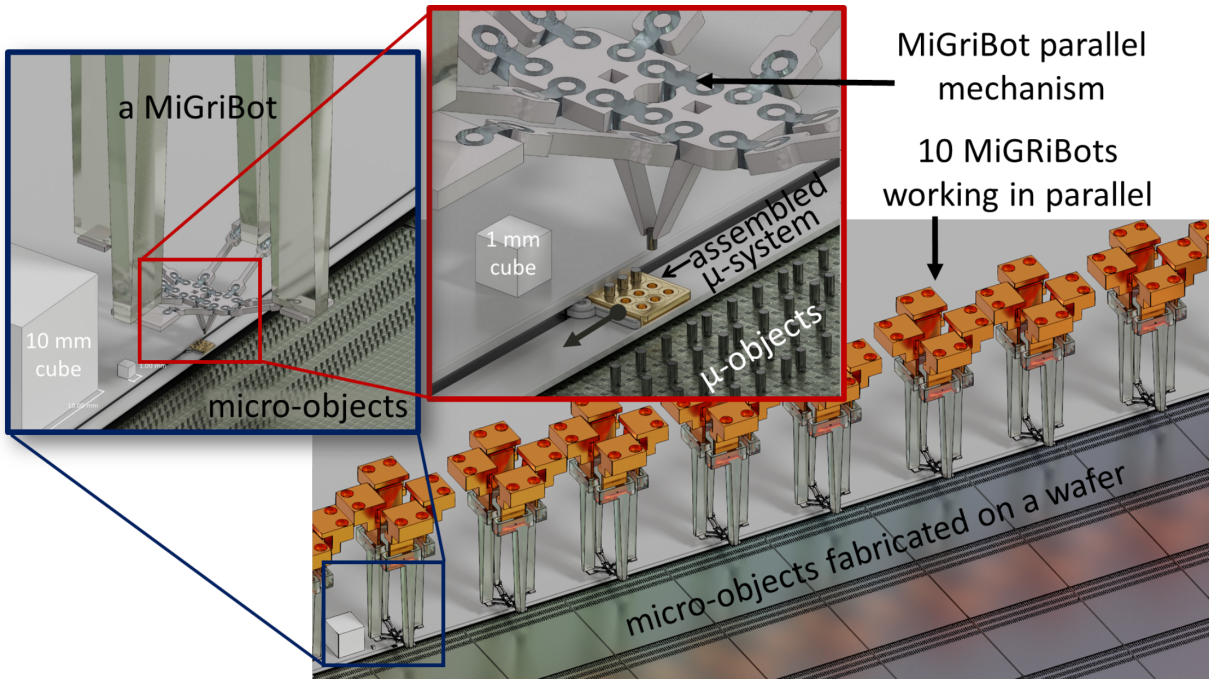

Fig. S7. Illustration of a parallel micro-assembly line using several MiGriBots. Beyond some advantages regarding the energy consumption, the compactness of MiGriBot enables to create a microfactory where several MigriBot would work in parallel on the same wafer increasing the global throughput by an order of magnitude. Each MiGriBot will be able to pick and place micro-objects with a 10 object per second throughput. Having 10 robots working in parallel enables to reach a global throughput of 100 objects per second.